Deep Learning-Based Minute-Scale Digital Prediction Model of Temperature-Induced Deflection of a Cable-Stayed Bridge: Case Study

Zi-xiang Yue[1]; You-liang Ding, Ph.D.[2]; and Han-wei Zhao, Ph.D., A.M.ASCE[3]

Abstract: The evolution rule of temperature-induced deflection in main girders is an important index to evaluate the service performance of long-span cable-stayed bridges, which directly reflects the coupling effect between the vertical stiffness of the main girder and the tension of multiple cables. However, temperature-induced deflection is caused by the complex temperature field of the main girder, cable tower and cable, while monitoring data have documented a time-lag effect between the temperature and temperature-induced deflection. Hence, it is difficult to accurately describe and model the behavior of the temperature-induced deflection in a long-span cable-stayed bridge in service. To this end, by utilizing the advantage of long short-term memory (LSTM) network for time series prediction, a digital model in minute scale based on monitoring data and deep learning can be developed to predict temperature-induced deflection, and resolve the low precision caused by the single-point input and time-lag effect. Compared with traditional machine learning algorithm and linear regression, a deep learning LSTM network has the best performance. For the cable-stayed bridge in this paper, the mean absolute error of the LSTM model was even less than 0.5 mm, and with the combined hypothesis test, the early warning accuracy for the abnormal change of temperature-induced deflection could achieve a minimum of 0.3%. **DOI: 10.1061/(ASCE)BE.1943-5592.0001716**. © *2021 American Society of Civil Engineers*.

Author keywords: Temperature-induced deflection; Cable-stayed bridge; Deep learning; LSTM; Digital model of prediction.

Introduction

As the main type of long-span bridges, the cable-stayed bridge is an indispensable link in the lifeline of transportation and has been applied extensively and increasingly (Zhou and Zhang 2019). Damage to the cables or main girder of cable-stayed bridges will lead to traffic interruption and even safety accidents (Malomo et al. 2020), resulting in serious economic losses (Kim et al. 2013); therefore, ascertaining the state of the cables and main girder is an important project of bridge operation and maintenance (Li and Ou 2015). Under the effect of temperature, the main girder of a cable-stayed bridge will produce significant vertical displacement, that is, temperature-induced deflection. Temperature-induced deflection is often more substantial than that caused by other effects (Zhu and Meng 2017). The deflection of the main girder of a cable-stayed bridge is an intuitive reflection of structural stiffness and the cable state (Wang and Ye 2019). To obtain the reference value of the temperature-induced deflection when a bridge operates under normal conditions, the modeling of the temperature field and temperature-induced deflection of the bridge has been an area of widespread concern.

Structural health monitoring (SHM) systems have been widely installed on long-span bridges, providing sufficient data regarding the environmental temperature and bridge response, so that research on bridge temperature effects based on data-driven analyses could be carried out (Sun et al. 2019). The static and dynamic responses of bridges are often significantly related to temperature (Xu et al. 2010; Ding and Li 2011). For a cable-stayed bridge, the main girder stress, cable tension, and displacement between towers emerge as linear correlations with temperature (Cao and Wang 2010; Yang et al. 2018a; Chen et al. 2017). The same phenomenon exists in the deflection and temperature of the main girder in cable-stayed bridges. However, a large error occurs when establishing the temperature-induced model through linear regression (Yang et al. 2018b), leading to findings that are still far from practical requirements.

On the other hand, the research has focused on the interaction mechanism of temperature-induced deflection and established the temperature-induced deflection model based on this mechanism. Temperature-induced deflection is caused by the temperature field acting on the main girder, cables, and towers of a cable-stayed bridge, and the temperature on the main girder is shown to be the primary factor for temperature-induced deflection, but the deflection caused by other temperature factors is also considerable after superposition (Zhou and Sun 2019a, b). However, the distribution of the temperature field of a cable-stayed bridge is exceedingly complex, given that the accuracy of the mechanism model is still insufficient. Depending on the detailed measured data and the finite element method, the temperature-induced mechanism has been further refined, improving the accuracy of the mechanism (Xu et al. 2019). Nevertheless, this method requires exceedingly complete bridge temperature information, and the operation process is complicated. On the other hand, a higher accuracy is still necessary if the model will be used in cable state recognition and other scenarios (Li and Chen 2019).

[1]Ph.D. Student, School of Civil Engineering, Key Laboratory of C&PC Structures of the Ministry of Education, Southeast Univ., Nanjing 210096, China. Email: viscarialight@126.com

[2]Professor, Key Laboratory of C&PC Structures of the Ministry of Education, Southeast Univ., Nanjing 210096, China (corresponding author). ORCID: https://orcid.org/0000-0002-0774-426X. Email: civilchina@hotmail.com

[3]Assistant Professor, Key Laboratory of C&PC Structures of the Ministry of Education, Southeast Univ., Nanjing 210096, China. ORCID: https://orcid.org/0000-0002-7622-7784. Email: wudizhw_0@126.com

Note. This manuscript was submitted on September 14, 2020; approved on January 8, 2021; published online on March 25, 2021. Discussion period open until August 25, 2021; separate discussions must be submitted for individual papers. This paper is part of the ***Journal of Bridge Engineering***, © ASCE, ISSN 1084-0702.

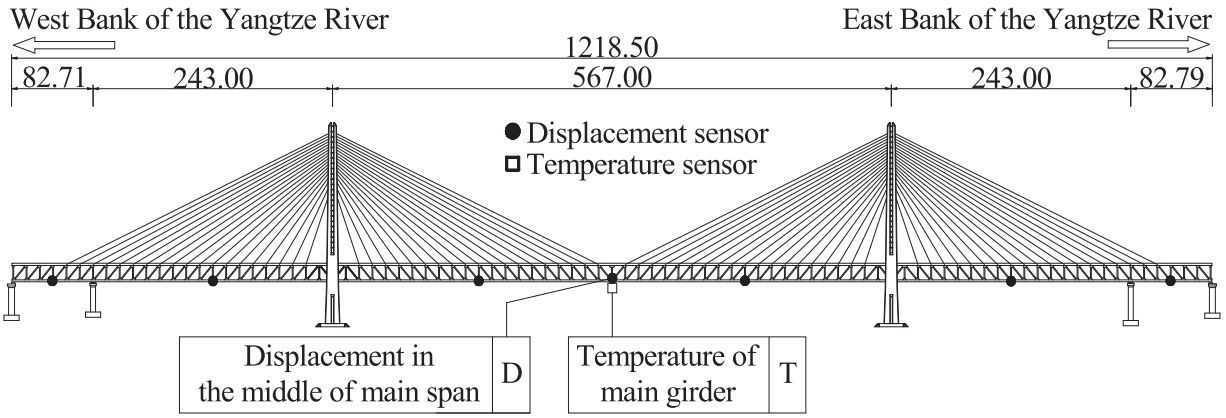

Fig. 1. Elevation of the bridge.

Health monitoring systems obtains the big data of bridge information, so machine learning can be used in bridge engineering, which introduces a new method for modeling the ambiguous and nonlinear relationship between environmental excitation and structure response (Ye et al. 2019; Sun et al. 2020). The support vector machine (Chaudhuri et al. 2018; Yang et al. 2014) and neural network (Jiao et al. 2014; Kaloop and Li 2014) have been widely used in predicting the temperature-induced effect of diverse buildings, achieving satisfactory effects. Because a cable-stayed bridge is a high-order statically indeterminate structure and the temperature field distribution is complex, it is necessary to study how to utilize machine learning technology in modeling the temperature-induced deflection of cable-stayed bridges.

Deep learning is the new branch of machine learning, which has better performance in dealing with highly nonlinear issues (Ye et al. 2019; Sun et al. 2020). The long short-term memory (LSTM) network is a kind of deep learning method, with especial effect for dealing with time series issues (Seep and Jurgen 1997). In bridge engineering, LSTM network has achieved good results in identifying vehicle loads and modeling wind-induced action (Zhao et al. 2020a; Li et al. 2020). Compared with traditional machine learning, the deep learning LSTM network is anticipated to have a better effect in a time series prediction model.

The temperature and temperature-induced deflection of a cable-stayed bridge are both quasistatic time series (Xu et al. 2019), and the possible temporal correlation in quasistatic time series will be the research basis in this paper. According to the temperature and deflection data of a typical long-span cable-stayed bridge, this paper will use the deep learning LSTM network to build a digital prediction model of temperature-induced deflection, and to map the nonlinear relationship between temperature and deflection. The result of the LSTM network will be compared with that of machine learning and linear regression to confirm the high performance of the LSTM. Finally, the purpose of this paper is to achieve high-precision output of temperature-induced deflection and to conduct exploration of an abnormal deflection warning on a cable-stayed bridge.

Monitoring of Bridge Temperature-Induced Deflection Behavior

Bridge Monitoring System

The monitoring data comes from of a steel truss girder cable-stayed bridge in the middle reaches of the Yangtze River. As a cable-stayed bridge with two towers and two cable planes, this bridge connects the east and west banks of the Yangtze River. The bridge is one of the largest combined highway and railway cable-stayed bridges in the world and is subjected to enduring train, vehicle, temperature, and other environmental actions. The concrete bridge towers are 193.5 m high with an "H" cross section. The main girder is continuous steel truss. The total length of this bridge is 1,218.5 m, and the main span is 567 m. As shown in Fig. 1, seven vertical deflection sensors are installed in the main girder of the bridge. The deflection data from the sensor in the middle of the main span will be used in the following study, for convenience, abbreviate this sensor as *D*. The temperature sensor of the main girder is in the nearby area, and the temperature sensor is abbreviated as *T*. As shown in Fig. 2, both *D* and *T* are located at the joint of the lower chord and are only installed on the upstream side; both *D* and *T* are 0.3 m downstream from the weld root of the web member and chord; *D* is aligned with center line of the vertical web member and *T* is 1 m east from the center line. The sampling frequency of both *D* and *T* is 1 Hz.

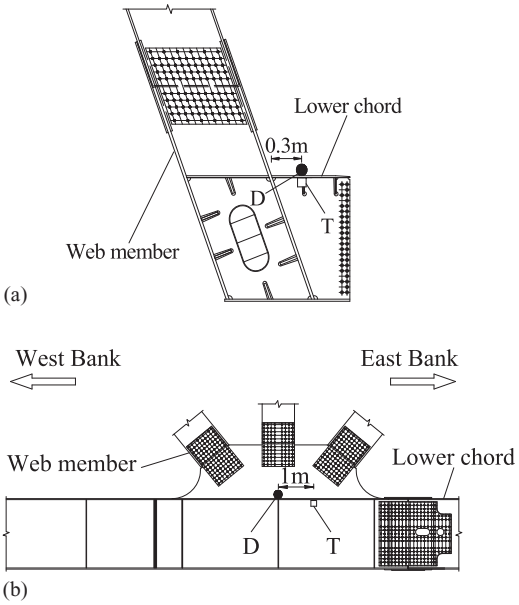

Fig. 2. Location of the sensors in the main girder: (a) front view; and (b) side view.

The temperature factors affecting the temperature-induced deflection are complicated, but the main factors are: (1) cable

temperature; (2) average temperature of main girder; (3) vertical temperature gradient in main girder; and (4) average temperature of two towers (Zhou and Sun 2019b). For this bridge, there is only one temperature monitoring point at the lower chord joint. As shown in Fig. 3, only the average temperature of the main girder can be approximately obtained by T; the other temperature information is unavailable.

Characteristics of Temperature-Induced Deflection

Fig. 4(a) shows the vertical displacement measured by sensor D on September 4, 2015. In the original data, the temperature-induced deflection exhibits a low-frequency trend similar to a sine wave. The high-frequency signal is the deflection caused by vehicles and trains, which fluctuates with the temperature deflection trend and resembles spikes. The deflection induced by vehicles is mostly less than 10 mm, and the deflection induced by trains is approximately 30 mm. The variation value of temperature-induced deflection in a single day is close to 30 mm and even more, which is also an important index to judge the state of the bridge. The research in this paper is based on temperature-induced deflection, so vehicle and train deflection need to be excluded. Extracting temperature-induced deflection is therefore the first step.

The extraction of the temperature-induced effect is normally carried out through hourly averaging (Yang et al. 2018b; Zhou and Sun 2019b; Xu et al. 2019). However, the research shows that the temperature-induced effect of a bridge does not change significantly within 10 min (Sun and Zhao 2019). In order to keep sufficient information and a reasonable data scale, in this paper, 10-min averages were preliminarily used to process the deflection data. In Fig. 4(a), the curve "10 min averaged" is the temperature-induced deflection.

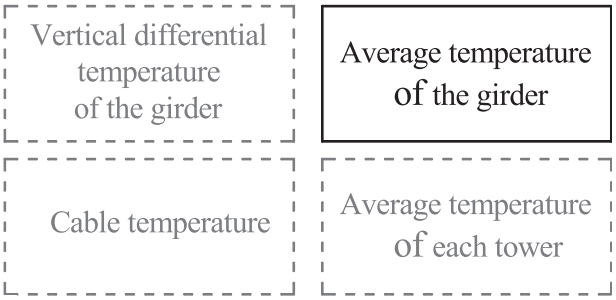

Fig. 3. Main reasons for temperature-induced deflection.

From Fig. 4(a), the dynamic residuals can still be observed in the temperature-induced deflection, so wavelet decomposition is used to further refine the low-frequency feature from the 10 min averaged results. As shown in Fig. 4(b), the "10 min averaged & wavelet filtered" curve is smoother and more accurately reflects the real situation, so the modeling accuracy will be improved (Liu et al. 2010).

The temperature-induced deflection data obtained by "10 min averaged and wavelet filtered" are named D. Correspondingly, the temperature data obtained by sensor T are also averaged by 10 minutes, and the averaged temperature data are named T. Fig. 5 shows D and T from February 1, 2015 to December 31, 2015. In Fig. 5, there is a negative correlation between D and T, that is, the height of the midspan will rise if the temperature of main girder increases.

Affected by the bridge deck, the upper part of the main girder usually heats up faster, which will cause a structural response earlier than that in the lower part (Wang and Ding 2019). Quantifying the time-lag effect as time differences could make the study convenient. According to the peaks and troughs of D and T, two time differences can be determined; the former time differences is named TL_1, and the latter is named TL_2. As shown in Fig. 6(b), due to the time-lag effect, the correlation scatter plot of "Oct. 23" is circular, resulting in a poor goodness of fit of the linear regression at only 0.494.

As shown in Fig. 7, the lag effect of "Nov. 30" is stronger than that of "Oct. 23", and the ring formed by the scatter plot is fuller because the goodness of fit is also worse, as low as 0.259. As shown in Fig. 8, on "Aug. 4", if TL_1 and TL_2 are very small, that is, the time-lag effect is inconspicuous, the scatter plot does not show a ring, and the goodness of fit is as high as 0.971.

Obviously, the weaker the time-lag effect is, the higher the accuracy of linear regression. According to the statistics of TL_1 and TL_2

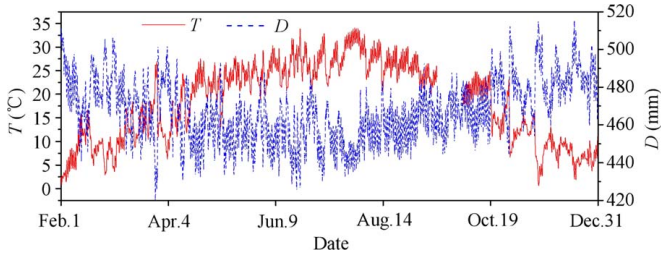

Fig. 5. Time histories of D and T.

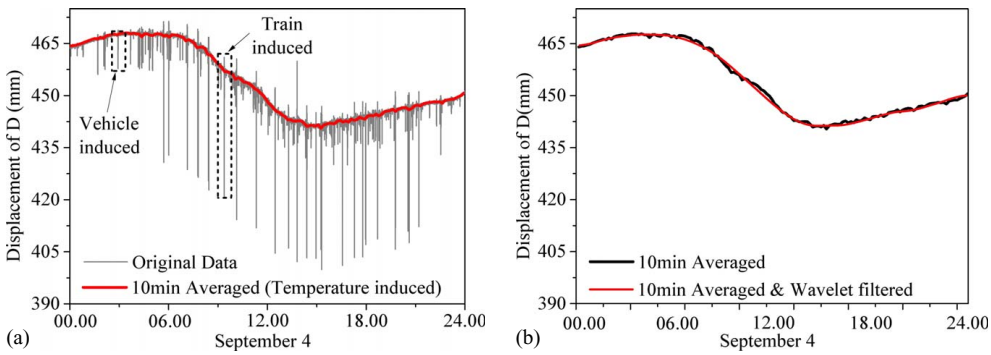

Fig. 4. Extraction of the temperature-induced deflection in the midspan: (a) original data and 10 min averaged data; and (b) 10 min averaged data and wavelet filtered data.

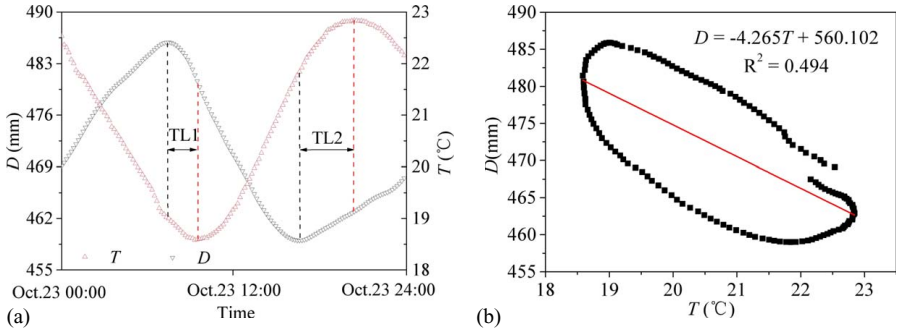

Fig. 6. Relationship between D and T on "Oct. 23": (a) time histories of D and T; and (b) scatter plot of D versus T.

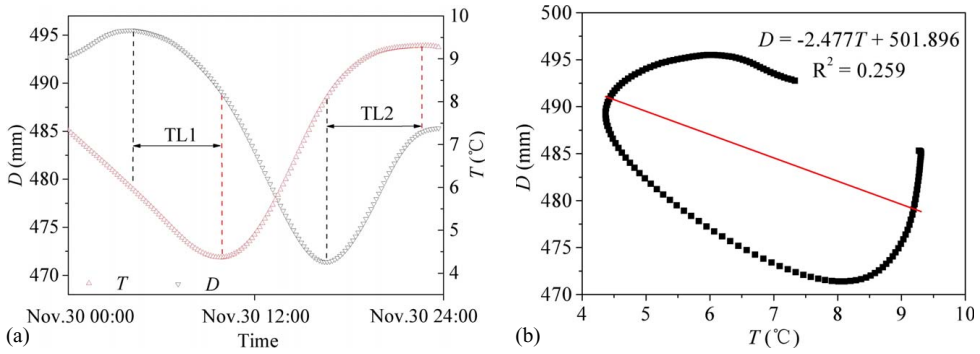

Fig. 7. Relationship between D and T on "Nov. 30": (a) time histories of D and T; and (b) scatter plot of D versus T.

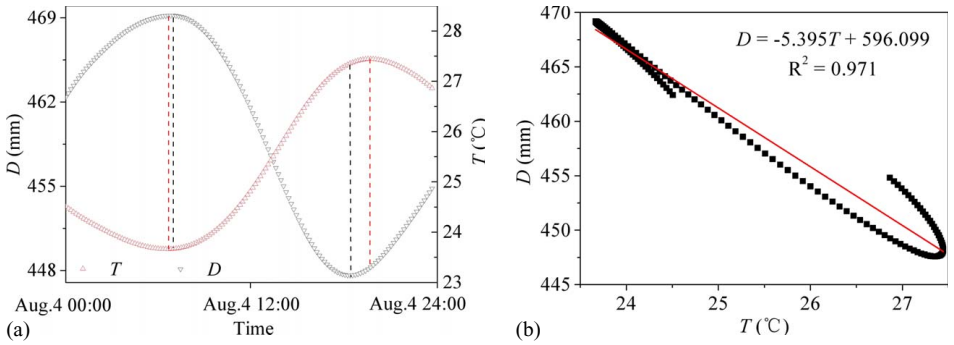

Fig. 8. Relationship between D and T on "Aug. 4": (a) time histories of D and T; and (b) scatter plot of D versus T.

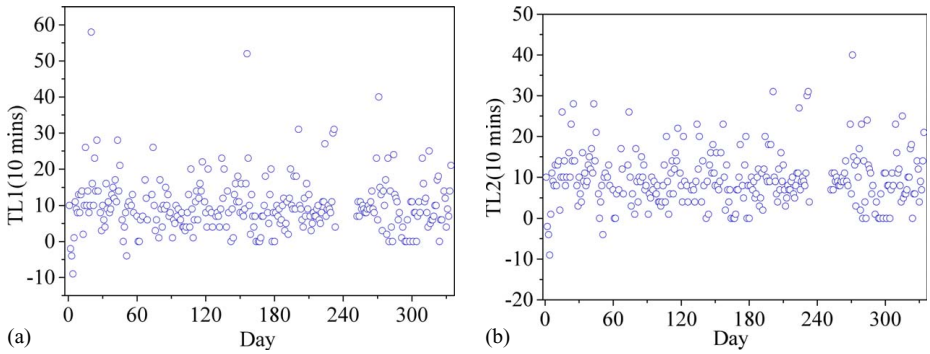

Fig. 9. Time differences caused by the time-lag effect: (a) TL_1; and (b) TL_2.

in each day of the 11-month data, as shown in Figs. 9(a and b), the time differences caused by time lags are divergent and have no obvious correlation with time history. Obviously, for large-scale data, the time-lag effect cannot be simply eliminated.

For the bridge monitoring data used in this paper, the time-lag effect and the incompleteness in temperature may negatively influence the modeling of the temperature-induced deflection. Linear regression will first be tried.

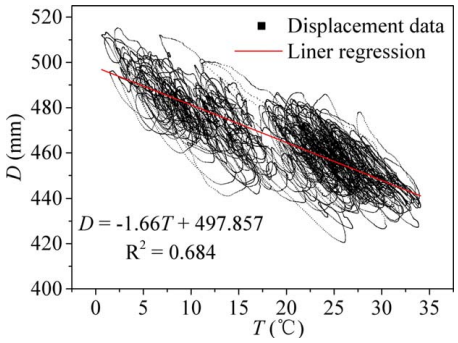

Fig. 10. Scatter plot of D and T.

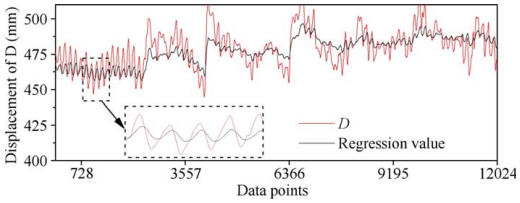

Fig. 11. Output result of linear regression model.

Linear Regression of Temperature-Induced Deflection

Fig. 10 shows the scatter plot of data for D and T over 11 months. The correlation between them is obvious, but the ring caused by the time-lag effect in a single day is still obvious. The linear regression model is $D = -1.66\,T + 497.857$, and the fitting goodness is only 0.684.

The last 25% of the data set are used for verification, bringing T into the linear regression equation, and comparing the regression result with the original data in Fig. 11. Only by observing the figure can it be seen that the regression result has a substantial error with regard to D in the amplitude and phase.

The following five indicators are used to measure the performance of the model.

MSE (Mean square error) as

$$\text{MSE} = \frac{1}{n}\sum_{n=1}^{N}(D_n - \hat{D}_n)^2 \tag{1}$$

where D_n = the measured value; $\hat{D}_n$ = the regression value; and N = the number of samples.

MAE (Mean absolute error) as

$$\text{MAE} = \frac{1}{n}\sum_{n=1}^{N}(D_n - \hat{D}_n) \tag{2}$$

MAX-AE (Maximum absolute error)

$$\text{MAXAE} = \max(D_n - \hat{D}_n) \tag{3}$$

MRE (Mean relative error)

$$\text{MRE} = \frac{1}{n}\sum_{n=1}^{N}\left(\frac{D_n - \hat{D}_n}{\hat{D}_n}\right) \tag{4}$$

MAX-RE (Maximum relative error),

$$\text{MAXRE} = \max\left(\frac{D_n - \hat{D}_n}{\hat{D}_n}\right) \tag{5}$$

Table 1 lists the error of the linear regression result. As shown, although MAE is only 6.7 mm and MRE is less than 2%, a higher accuracy is still required in some application scenarios. MAX-AE is more than 20 mm, and MAX-RE is more than 5%, which is considerably different from the average value. Meanwhile, MSE is more than 70 mm, which is 10 times greater than MAE, showing that the deviation between the predicted result and the measured result is not stable. By solely using the temperature of the main girder, the accuracy and stability of the predicted result by linear regression is relatively poor, not achieving the reliability required by engineering applications.

Table 1. Kinds of error of linear regression results

Kind	MSE
MSE	71.40 mm
MAE	6.70 mm
MAX-AE	27.28 mm
MRE	1.40%
MAX-RE	5.35%

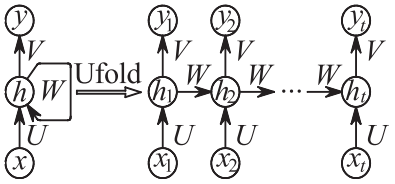

Fig. 12. Common architecture of RNN.

Digital Prediction Model for Temperature-Induced Deflection

Because of the single-point temperature input and time-lag effect, linear regression encounters difficultly in fitting a high-precision temperature-induced deflection model. Deep learning, a branch of machine learning, has an excellent effect in ambiguous and nonlinear modeling. The digital prediction model of temperature-induced deflection will be established by a deep learning LSTM network, in order to overcome the disadvantages of linear regression. Moreover, the wavelet neural network (WNN), a general machine learning method, is used for comparison as evidence that the deep learning method is more suitable for modeling temperature-induced deflection.

Deep Learning LSTM Network

The recurrent neural network (RNN) is a deep neural network often used in time series models. Different from other neural networks, RNN develops the connection between nodes in the hidden layer, enabling an RNN to display the dynamic behavior of a time sequence and use its internal state to process the input sequence (Graves et al. 2009). The common RNN architecture is shown in Fig. 12.

The RNN structure with time flow is shown in Fig. 12. For a given input sequence $\boldsymbol{x} = (x_1, x_2, \ldots, x_{t-1}, x_t)$, hidden layer sequence $\boldsymbol{h} = (h_1, h_2, \ldots, h_{t-1}, h_t)$, and the output sequence $\boldsymbol{y} = (y_1, y_2, \ldots, y_{t-1}, y_t)$. The relational expression is shown as

$$h_t = f(\boldsymbol{U}x_t + \boldsymbol{W}h_{t-1} + \boldsymbol{b}_h) \tag{6}$$

$$y_t = \boldsymbol{V}h_t + \boldsymbol{b}_y \tag{7}$$

Eq. (6) represents the hidden layer, which is a recursive layer, where f = the activation function; $\boldsymbol{U}$ = the weight matrix of input

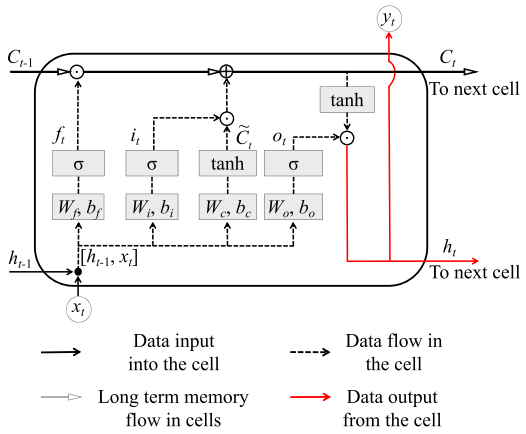

Fig. 13. Structure of a cell in the LSTM network.

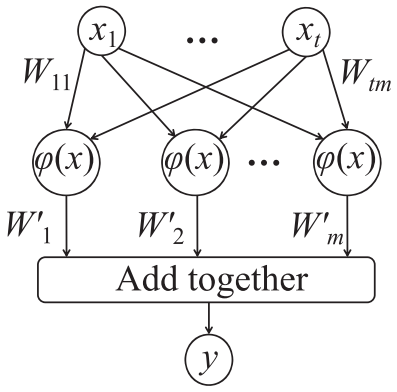

Fig. 14. Common architecture of the WNN.

x_t; $\boldsymbol{W}$ = the weight matrix of the previous h_{t-1}; and $\boldsymbol{b}_h$ = the bias vector. Eq. (7) represents the output layer, which is the fully connected layer, where $\boldsymbol{V}$ = the weight matrix of output h_t; and $\boldsymbol{b}_y$ = the offset vector.

It can be seen from Eqs. (6) and (7) that the output of an RNN is affected by the input at the current time and the result of recursive layer at the previous time, meaning that RNN can learn the logic of the time sequence, so it has a unique advantage in prediction. However, when the traditional RNN is dealing with long sequences, the problem of gradient explosion or gradient disappearance will appear in the model training phase (Yoshua et al. 1994), which limits the memory ability for long sequences.

The LSTM network is a kind of improved RNN, which uses the memory unit with a gate structure to replace the neurons in the hidden layer, thus alleviating the problem of gradient disappearance. Therefore, LSTM is highly suitable for the prediction of time series with nonlinear input–output relationship (Seep and Jurgen 1997; Gers and Schmidhuber 2000). Practice has proven that the LSTM has a high performance in time series problems for bridge engineering (Zhao et al. 2020b; Li et al. 2020).

Fig. 13 shows a memory unit of the LSTM network, where $\boldsymbol{f}_t$, $\boldsymbol{i}_t$, and $\boldsymbol{o}_t$ = forget gate, input gate, and output gate respectively; $\sigma(z)$ and $\tanh(z)$ = the activation functions, $\sigma(z)$ is described by logistic sigmoid, and $\tanh(z)$ is described by hyperbolic tangent sigmoid, and the range of z is $[-1, 1]$; $\boldsymbol{W}_f$, $\boldsymbol{W}_i$, $\boldsymbol{W}_C$, $\boldsymbol{W}_o$ and $\boldsymbol{b}_f$, $\boldsymbol{b}_i$, $\boldsymbol{b}_C$, $\boldsymbol{b}_o$ = the corresponding weight matrices and biases vectors; x_t = the input at time t; h_t = the cell output; and C_t and $\tilde{C}t$ = the cell state and internal hidden state, respectively. This can be represented as

$$\text{Forget gate: } \boldsymbol{f}_t = \sigma(\boldsymbol{W}_f[h_{t-1}, x_t] + \boldsymbol{b}_f) \tag{8}$$

$$\text{Input gate: } \boldsymbol{i}_t = \sigma(\boldsymbol{W}_i[h_{t-1}, x_t] + \boldsymbol{b}_i) \tag{9}$$

$$\text{Candidate memory unit: } \tilde{\boldsymbol{C}}_t = \tanh(\boldsymbol{W}_C[h_{t-1}, x_t] + \boldsymbol{b}_C) \tag{10}$$

$$\text{Current time memory unit: } \boldsymbol{C}_t = \boldsymbol{f}_t \cdot \boldsymbol{C}_{t-1} + \boldsymbol{i}_t \cdot \tilde{\boldsymbol{C}}_t \tag{11}$$

$$\text{Output gate: } \boldsymbol{o}_t = \sigma(\boldsymbol{W}_o[h_{t-1}, x_t] + \boldsymbol{b}_o) \tag{12}$$

$$\text{Output: } \boldsymbol{h}_t = o_t \cdot \tanh(C_t) \tag{13}$$

$$\sigma(z) = \frac{1}{1 + e^{-z}} \tag{14}$$

$$\tanh(z) = \frac{e^z - e^{-z}}{e^z + e^{-z}} \tag{15}$$

Eqs. (8)–(15) basically describe the forward pass of the LSTM. As shown, the structure of LSTM is elaborate, so it can control the reservation degree of the existing information in the current network cell, the integration degree of the existing information, and the input information at the current time; in addition, the information that will be inputted to the unit at the next time will also be preprocessed in the current unit.

The neural network algorithm has a back-propagation process, that is, using the error of the output result in each iteration, the gradient of the loss function can be calculated in the network; then, the internal parameters of the neural network are constantly modified. The back-propagation through time (BPTT) algorithm can help the LSTM network to complete gradient descent (Williams and Peng 1990) and finally obtain a model with high accuracy.

The temperature-induced deflection is a quasistatic time series having negative correlation with the main girder temperature and an obvious nonlinear regularity with time. At the same time, there is time lag between the girder temperature and temperature-induced deflection, and the distribution of the time-lag values is irregular.

Establishing the model of temperature-induced deflection is to clarify the complex relationship between the two time series of the temperature-induced deflection and girder temperature. Therefore, this paper uses the LSTM network to build the digital prediction model to clarify the ambiguous and nonlinear mapping relation between the girder temperature and temperature-induced deflection. Finally, elimination the time-lag effect is achieved and the high-accuracy output of the deflection is obtained.

Machine Learning WNN

To prove the excellent performance of the deep learning LSTM network, it will be compared with the traditional machine learning neural network. The WNN is the machine learning algorithm improved from back-propagation (BP) neural network. Different from the BP neural network, the excitation function of the hidden layer in the WNN is replaced by a wavelet function (Zhang 1992). Compared with the general BP neural network, the WNN is more suitable for modeling nonlinear issues (Chen et al. 1999). The structure of the WNN is shown in Fig. 14.

In Fig. 14, x_1, …, x_t = the input information; W_{tm} = the weight coefficient between the input layer and the hidden layer; $\varphi(x)$ = the wavelet basis function in the hidden layer; W'_m = the weight coefficient of the output information; and y = the final output from the information after dimension reduction and integration.

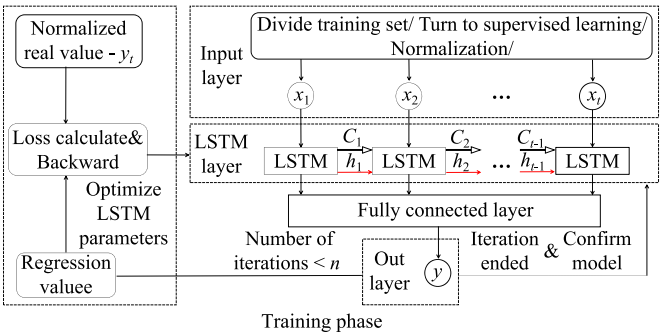

Fig. 15. Training flow of LSTM network (n is the specified number of iterations).

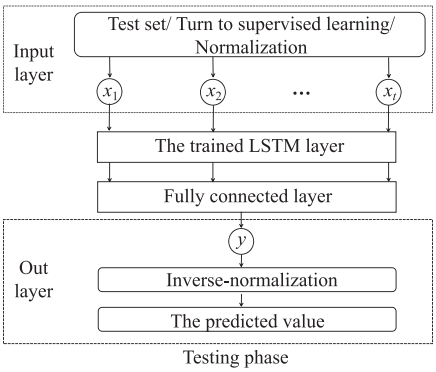

Fig. 16. Test flow of LSTM network.

In this paper, the WNN and LSTM will be used to establish the time series prediction model of temperature-induced deflection by comparing the output results to confirm the advantage of the deep learning LSTM over the traditional machine learning network, to find the best temperature-induced deflection modeling method. Because this paper mainly focuses on the LSTM network and the building process of the neural network is similar, the building process of the WNN will not be introduced in detail.

Building Process of the Digital Prediction Model

The modeling is based on PyTorch, which is the Python machine learning package. For two time history data samples $\boldsymbol{X}$ and $\boldsymbol{Y}$, when using the time sequence $\{X_1, X_2, \ldots, X_t\}$ to predict the value Y_t at time point t, the mapping relationship between them can be established by the LSTM network. The building process of the LSTM network can be divided into two phases: training and testing. Fig. 15 shows the training phase and structure of the LSTM network, which can be roughly divided into five parts: (1) input layer, (2) LSTM layer, (3) fully connected layer, (4) output layer, and (5) optimization module. This paper will introduce the training phase from these five parts.

Input Layer

As shown in Fig. 15, the original data should first be divided into the training set and test set. Generally the top 75% of the data are used as the training set, and the last 25% of the data are used as the test set. After that, the data should be reformed into the supervised learning type. Supervised learning is a machine learning task that infers a function from labeled training data. In supervised learning, the data type is that an input sequence corresponds to a desired output value.

Because the activation function of the neural network requires an input range [0, 1], so the data need to be normalized. The following is the normalization formula, and $\{x_1, x_2, \ldots, x_t\}$ is the normalized input sequence from time 1 to time t:

$$x_t = \frac{X_t - X_{\min}}{X_{\max} - X_{\min}} \tag{16}$$

where X_t = the value at time t; $X_{\max}$ = the maximum value in sample $\boldsymbol{X}$; and $X_{\min}$ = the minimum value in sample $\boldsymbol{X}$.

LSTM Layer

As shown in Fig. 15, $\{x_1, x_2, \ldots, x_t\}$ will be brought into the LSTM network for forward propagation. The propagation flow in the LSTM unit is shown in Fig. 13. The data will be output after passing through the LSTM unit.

Fully Connected Layer

As shown in Fig. 15, the values output by the LSTM are not the expected single value but a series of values. The function of the fully connected layer is to integrate the values from the LSTM layer, obtaining a single value.

Output Layer

As shown in Fig. 15, after the integration of the fully connected layer, we can map the value y, that is, the regression value of the model. It should be emphasized that y is only the value used in training the network and is not yet the deflection value.

Optimization Module

As shown in Fig. 15, y = the regression value mapped by normalized input data $\{x_1, x_2, \ldots, x_t\}$, so the range of y is [0,1]. A preset number of iterations is specified as n. Before iterations reach the number n, the MSE is calculated by each regression value and the real value can be used as the loss function to carry out BP and update the internal parameters of the LSTM network, and finally complete gradient descent. Because y is the normalized value, the real value Y_t should also be normalized in train phase, and the normalization principle is

$$y_t = \frac{Y_t - Y_{\min}}{Y_{\max} - Y_{\min}} \tag{17}$$

where y_t = the normalized real value; Y_t = the value at time t; $Y_{\max}$ = the maximum value in sample $\boldsymbol{Y}$; and $Y_{\min}$ = the minimum value in sample $\boldsymbol{Y}$.

Iteration will stop when the specified number n is reached and the output error meets the requirement, which means that the LSTM model has completed the training.

Fig. 16 is the test phase of the LSTM network in this paper. In the input layer, the test set is the last 25% of the data that are independent of the training test set. After transforming the data into the supervised learning form and normalizing the data, the data are brought into the LSTM layer that has completed the training. After the integration of the full connection layer, the regression value y is output. Here, y = the normalized value, through the inverse normalization; then, the predicted data Y_p mapped by input data can be obtained. The inverse normalization is shown as

$$Y_p = (Y_{\max} - Y_{\min})y + Y_{\min} \tag{18}$$

where Y_p = the regression value through inverse normalization, that is, the predicted value; and y = the regression value before inverse normalization.

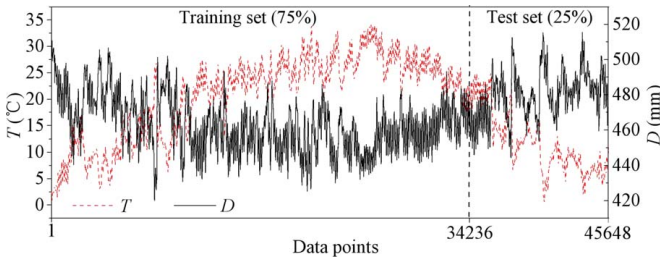

Fig. 17. Test set and training set.

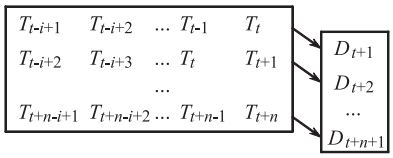

Fig. 18. Mapping relationship between input and output data utilizing time correlation.

Table 2. Hyperparameters of WNN and LSTM networks

Type of neural network	Type of hyperparameter	Value/ characteristic
Hyperparameters of LSTM	Number of cells in input layer (Time steps)	i
	Input_size	1
	Batch_size	10
	Learning rate	0.0001
	Number of cells in LSTM layer	64
	Number of cells in fully connected layer	64
	Number of cells in output layer	1
	Training iterations(epoch)	100
Hyperparameters of WNN	Number of cells in input layer (Time steps)	i
	—	—
	Batch_size	10
	Learning rate	0.0001
	Number of cells in hidden layer	64
	Number of cells in fully connected layer	64
	Number of cells in output layer	1
	Training iterations(epoch)	100

Modeling Temperature-Induced Deflection Based on LSTM

After eliminating the blank values, Fig. 17 shows the data of T and D during February to December. The training set and test set are independently divided according to the proportions of 75% and 25%. There are 45,648 data points totally and 34,236 data points in the training set. Then, we develop the supervised learning strategy for building the neural network model.

Learning Strategy A: Temperature → Deflection

The time series of temperature and temperature-induced deflection are quasistatic and change slowly. At the same time, a significant time-lag effect exists between the two time series. Obviously, there is inertia in temperature-induced deflection, signifying there is correlation between the previous temperature series and the deflection value at the next moment. Using this idea, this paper develops learning strategy A, which uses a temperature data sequence as input corresponding the deflection data at the next moment as output to complete the prediction model of temperature-induced deflection. According to this learning strategy, the mapping relationship between temperature and deflection data over time is shown in Fig. 18.

In Fig. 18, the parameter i is the step number of the temperature data input, indicating the duration of the temperature inertia effects on temperature-induced deflection. Here, i is also the number of cells in the input layer of the neural network. When learning strategies are developed, we can start building neural networks. Considering that the mapping relationship to be implemented in this article is not complicated, according to the Kolmogorov theorem (Kurkova 1992), trials, and existing experience, the WNN and LSTM networks are set to one input layer, one hidden layer, one fully connected layer, and one output layer. The hyperparameters of WNN and LSTM networks are listed in Table 2. The number of cells in the input layer needs to be determined according to the number of time steps in the learning strategy. Consequently, the best number of i should first be determined.

The number of input steps from $i = 1$ (10 min) to $i = 144$ (1 day) are formulated. Bringing the data set into the WNN and LSTM networks and evaluating the output results by MSE, the results are shown in Fig. 19. It can be seen that $i = 30$ is the best number of input steps for the WNN or LSTM network.

In Fig. 20, the mapping relationship of learning strategy A is shown, inputting the previous 30 temperature data points to output the deflection data point at the next moment. The number of training iterations is 100, and as shown in Fig. 21, the error of the WNN and LSTM network is small after iterating. The training target is achieved, and a suitable model is obtained.

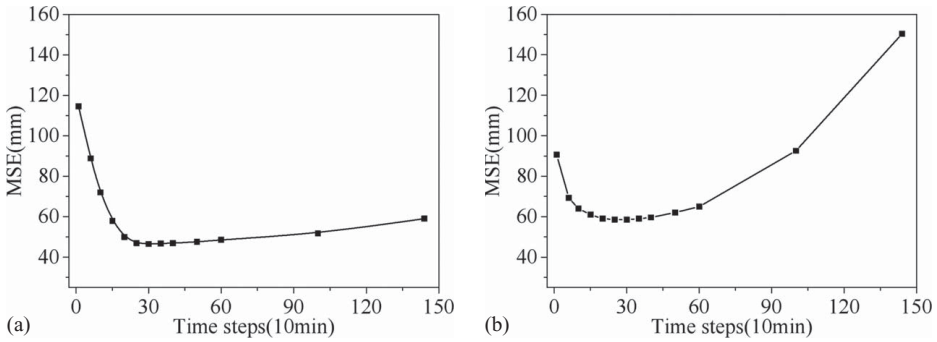

Fig. 19. Relation between input steps and output error: (a) WNN; and (b) LSTM.

First, the test set is brought into the trained WNN and the output result is compared with the original data as shown in Fig. 22. From Figs. 11 and 22, compared with the results by linear regression, the WNN automatically eliminates the phase error caused by the time-lag effect, and the amplitude error is also reduced.

Table 3 lists the error indexes of the output values of the test set using the WNN method. Compared with the result of linear regression in Table 1, each index was only slightly improved, having no qualitative change. At the same time, MSE is eight times higher than MAE, which indicates that the output is unstable and the reliability of this model is reasonable.

Then the test set is brought into the trained LSTM network, and the output results are compared with the original data as shown in Fig. 23. From Figs. 11 and 23, compared with the results of linear regression, the LSTM network can also automatically eliminate the phase error and reduce the amplitude error.

Table 4 lists the error indexes of the output values by the LSTM method. Compared with the result of linear regression in Table 1, each index is only slightly improved, also having no qualitative change. At the same time, the MSE is nine times higher than MAE, which indicates that the output result is unstable and the reliability of the model is low. When learning strategy A is used, the output error of the LSTM method is larger than that of the WNN method, not showing the expected advantage.

In conclusion, using learning strategy A that inputs temperature and outputs deflection, the WNN and LSTM network have better performance than linear regression, where not only the phase error is smaller but also the amplitude accuracy is higher. Obviously, machine learning can eliminate the influence of incomplete temperature information and the time-lag effect to a certain extent. However, using strategy A, the accuracy of two neural network models is still not satisfactory. A better learning strategy needs to be explored.

Learning Strategy B: Temperature + Deflection → Deflection

Owing to the temperature-induced deflection being caused by the complex temperature field, it is not enough to establish a high-precision model only by the main girder temperature. We have found that the temperature-induced deflection is a quasistatic series, similar to the temperature series that changes slowly with time. Therefore, we can be sure that the temperature-induced deflection series have temporal correlation, similar to the temperature series. The historical sequence of the temperature-induced deflection may be related to the data point itself at the next moment. According to this inference, historical deflection data were used to supplement the inadequate temperature information. Therefore, learning strategy B is formulated, inputting both the historical deflection

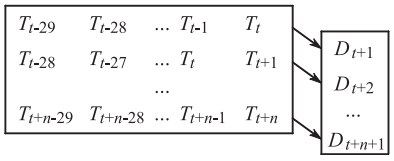

Fig. 20. Mapping relationship between input and output data by strategy A.

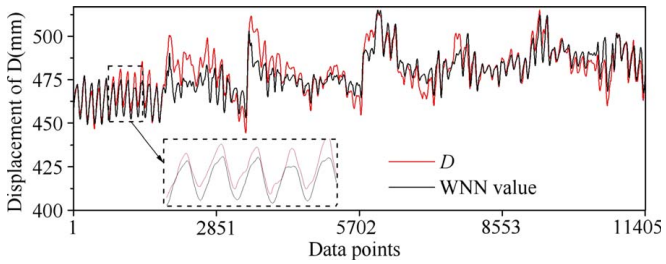

Fig. 22. Output result of WNN by strategy A.

Table 3. Kinds of error of WNN results by strategy A

Kind	MSE
MSE	46.53 mm
MAE	5.22 mm
MAX-AE	21.09 mm
MRE	1.08%
MAX-RE	4.22%

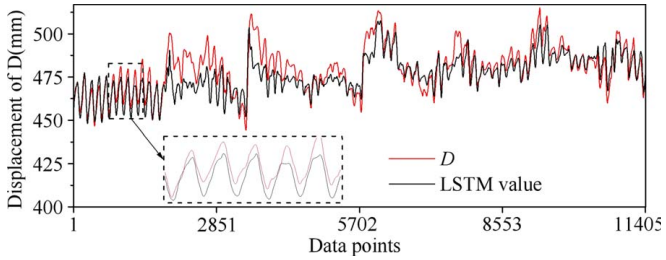

Fig. 23. Output result of LSTM network by strategy A.

Table 4. Kinds of error of LSTM results by strategy A

Kind	MSE
MSE	58.45 mm
MAE	5.85 mm
MAX-AE	24.20 mm
1 MRE	1.18%
MAX-RE	4.78%

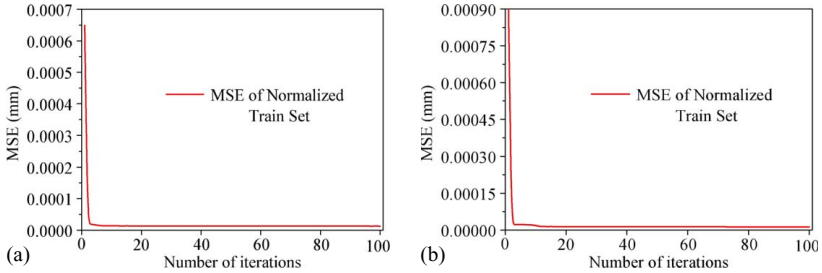

Fig. 21. Loss curves of neural networks by strategy A: (a) WNN; and (b) LSTM.

and temperature series, and the deflection data at the next moment are output. The number of input steps is 30, and the mapping relationship is shown in Fig. 24. As shown in Fig. 24(a), for LSTM network, when both D and T are input into networks, the two features need to be combined as one vector, and the input size should be increased to 2. As shown in Fig. 24(b), for WNN, the number of the cells in the input layer should be increased to 60. The other hyperparameters of the WNN and LSTM network do not change.

The number of training iterations is also 100 when using strategy B, and as shown in Fig. 25, the error of the WNN and LSTM network is small after iterating. The training target is achieved, and a suitable model is obtained.

The test set is brought into the trained WNN, and the output results are compared with the original data as shown in Fig. 26. From Figs. 26 and 22, the accuracy of strategy B is greatly improved compared with that of strategy A. However, the prediction accuracy of WNN decreases with the passage of time.

Table 5 gives the error indexes of the WNN output result by strategy B. Even though MAE is relatively small, MAX-AE is still quite different from MAE, and MSE is more than five times MAE, indicating that the reliability of the prediction is still not reasonable.

As shown in Fig. 27, the test set is brought into the trained LSTM network, and the output results are excellent; both phase error and amplitude error are extremely small. Only by observation, it can be determined that LSTM is the most accurate method among the several methods.

As presented in Table 6, the output error of the LSTM network is very low; when using strategy B, MAE is less than 1 mm and MRE is less than 0.1%. MAX-AE is only 2.98 mm and MAX-RE is only 0.58%; meanwhile MSE is even less than MAE, which illustrates that the output is stable, proving that the model has a high reliability.

Using the deep learning LSTM network with strategy B, the temperature-induced deflection model with good reliability and ultrahigh precision can be established, which is the best scheme. The purpose of establishing a high-precision temperature-induced deflection model is not only to output the reference value in normal states but also to realize the early warning of the abnormal bridge state finally. This paper will explore the application potential of the model.

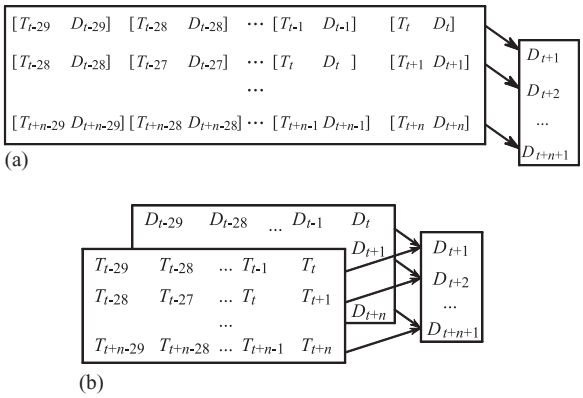

Fig. 24. Mapping relationship between input and output data by strategy B: (a) strategy B for LSTM; and (b) strategy B for WNN.

Model Application

Identification of Abnormal Deflection

The temperature-induced deflection of cable-stayed bridge is sensitive to the cable damage. If the cables are damaged in different degrees, temperature-induced deflection will vary from 2 to 20 mm, only accounting for 1%–10% of the normal deflection (Wang and Ye 2019; Ge and Su 2016), so it is difficult to identify extremely small abnormal deflection by ordinary methods. The LSTM network based on strategy B shows the advantage of high accuracy and the potential in identification of abnormal deflection. To further investigate the performance of this method applied in structural state early warning, imposing deviation on the deflection value of the test set to simulate the influence of structural damage is performed, and then the response of the model output is observed.

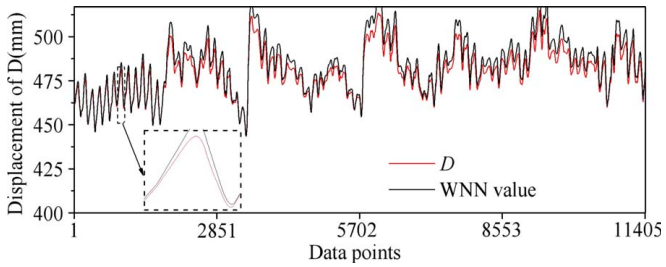

Fig. 26. Output result of WNN by strategy B.

Table 5. Kinds of error of WNN results by strategy B

Kind	MSE
MSE	22.96 mm
MAE	4.13
MAX-AE	12.82 mm
MRE	0.85%
MAX-RE	2.49%

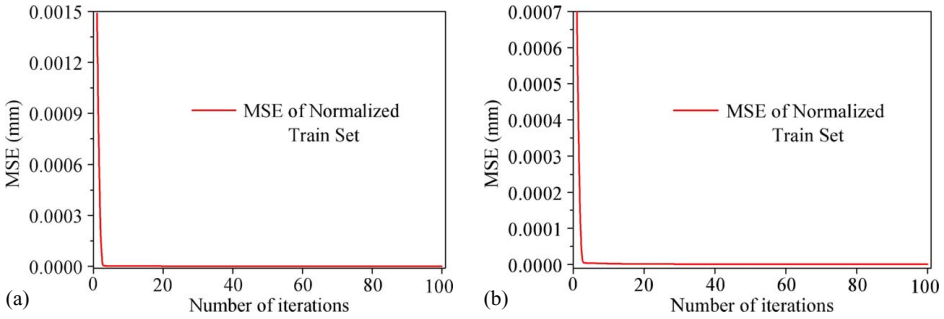

Fig. 25. Loss curves of neural network by strategy B: (a) WNN; and (b) LSTM.

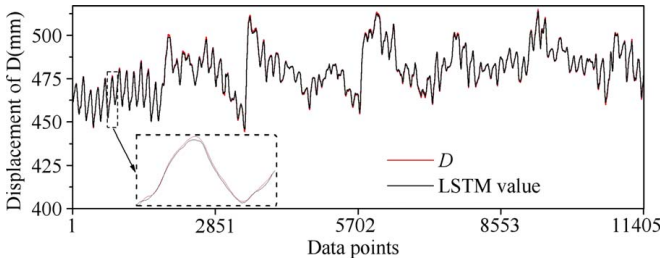

Fig. 27. Output result of LSTM network by strategy B.

Table 6. Kinds of error of LSTM results by strategy B

Kind	MSE
MSE	0.34 mm
MAE	0.45 mm
MAX-AE	2.98 mm
MRE	0.09%
MAX-RE	0.58%

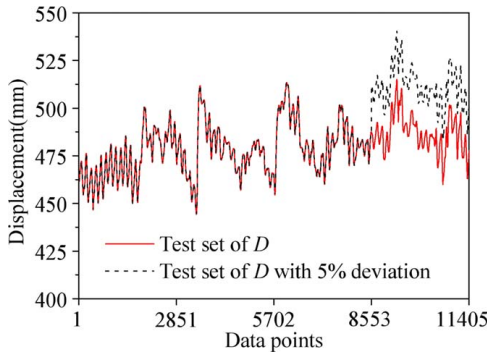

Fig. 28. Test set with deviation from 75%.

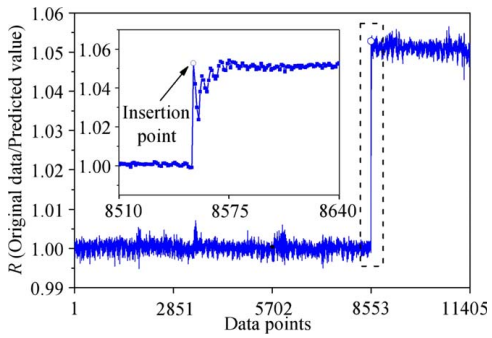

Fig. 29. Output of test set with deviation from the 75% position.

A 5% deviation is used for preliminary verification, and the deviation starts from 75% in the test set. The test set with deviation is shown in Fig. 28.

The test set with deviation is brought into the trained LSTM model. After obtaining the output result, the ratio of original value and predicted value is analyzed. For convenience, the ratio of original value and predicted value is referred to as R. The output result of that with deviation is shown in Fig. 29.

As shown in Fig. 29, when the deviation starts from 75%, because the learning strategy is to map the data at next moment, there is a ratio change immediately at the insertion point of the deviation. The R value is 1.053, which clearly indicates the deviation of 5%. Then, the data with deviation enter the historical data, which changed the time correlation characteristic of the input data. The output value suddenly increases and the ratio R decreases. With the deviation data continuously replacing the original data, the time correlation characteristic gradually returns to normal, and R gradually returns to 1.05.

To further explore the application potential of the model, from the 75% position of the test set, reducing the deviation percentage, the test set is processed with the deviation ratio of 2%/0.5%, and then the processed test set is brought into the trained LSTM model. The output results are shown in Fig. 30.

As shown in Fig. 30, with the decrease of the deviation, the model can still accurately identify the abnormal deflection, even if the deviation value is only 0.5%, it can be observed that R changes significantly.

According to the preceding information, it can be preliminarily determined that the model has the ability to identify the abnormal deflection. However, due to the vast amount of monitoring data and the fluctuation of the model output, for the early warning of abnormal deflection, the model lacks a mathematical basis by solely observing the ratio R, and the reliability will not be reasonable. The combination of the neural network and hypothesis test has a good effect for the bridge state early warning (Ding et al. 2010; Zhao et al. 2020b). Therefore, it is better to explore if combining the hypothesis test and LSTM model can achieve a good effect in the early warning of the abnormal structural state.

Structural Abnormal State Warning Based on Statistical Pattern Recognition

The ratio R is used as the early warning index to judge whether the structure deflection is abnormal. The output result is divided into two groups. The output result at the 25% position before the insertion point represents the normal state of the deflection, and the output result at the last 25% position with the deviation represents the abnormal state. Through the early warning index R, a t-test is used to compare whether the mean values of the two groups have a significant difference in order to achieve the purpose of the abnormal

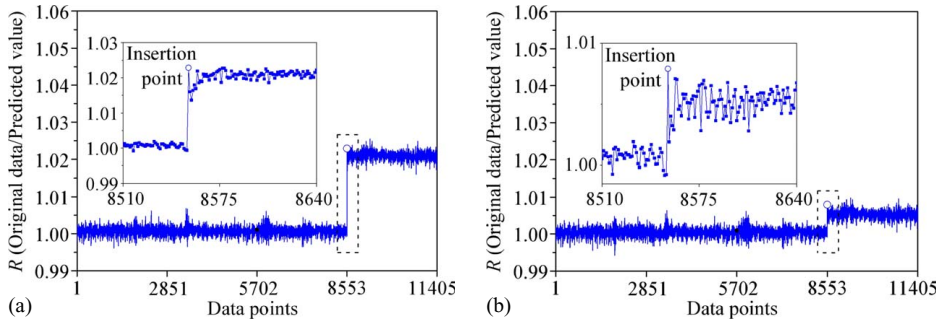

Fig. 30. Output of test sets with different deviations: (a) 2% deviation; and (b) 0.5% deviation.

Table 7. Abnormal state warning results

Deviation (%)	p value	t-test
2	0	H_1
1	0	H_1
0.5	0	H_1
0.4	0	H_1
0.3	0	H_1
0.29	0.041	H_1
0.28	0.052	H_0
0.27	0.066	H_0
0.26	0.082	H_0
0.25	0.102	H_0

state warning, which can be represented as

$$H_0{:}\mu_1 = \mu_2,\ H_1{:}\mu_1 \neq \mu_2 \tag{19}$$

where μ_1 and μ_2 = the mean values of R from the normal output result and the abnormal output result respectively.

As shown in Eq. (19), when the p value of t-test is less than 0.05, the test result is H_1, which indicates there is a significant difference between μ_1 and μ_2, that is, the structure state is abnormal. Otherwise, the result is H_0, indicating that the abnormal state was not identified. The deviation is reduced from 2% to 0.25%. Table 7 gives the t-test results under different deviations.

As presented in Table 7, the minimum abnormal change of deflection that can be identified is 0.3%, which shows that the temperature-induced deflection model established by LSTM has excellent damage sensitivity and early warning ability.

Conclusion

Taking the advantage of the deep learning LSTM network in time series modeling, a high-precision digital prediction model of temperature-induced deflection is established. The application of this model in identifying abnormal deflection is studied through the hypothesis test and the main conclusions are shown as follows:

1. A time-lag effect exists between the temperature-induced deflection and temperature data. The time lag in each day is complex and cannot be easily eliminated. Owing to the incompleteness of temperature information and the time-lag effect, the minute-scale regression model of temperature-induced deflection solely based on the main girder temperature has a large error in phase and amplitude.
2. By using the WNN and LSTM network, the digital prediction model that inputs the time series of the main girder temperature and outputs the deflection data at the next moment is established. Compared with the linear regression result, for the results of the WNN and LSTM, the phase error caused by the time lag is eliminated, however, the amplitude error is still very large.
3. By inputting the time series data of temperature and deflection together. The output deflection not only eliminates the time log but also greatly reduces the amplitude error caused by incomplete temperature information. Compared with machine learning WNN, the deep learning LSTM network has ultrahigh precision. When applied to the bridge in this paper, the average error of the digital model is less than 0.5 mm.
4. Based on the output result of the LSTM model and combining the hypothesis test, deflection anomalies at more than 0.3% can be identified, verifying the potential of the model in bridge early warning.

The temperature-induced deflection of the main girder on cable-stayed bridge is the intuitive expression of structure stiffness and cable state. The application of this model in bridge operation and maintenance will be further studied.

Data Availability Statement

All of the data, models, or codes that support the findings of this paper are available from the corresponding author upon reasonable request.

Acknowledgments

This research was supported by the Fund for Distinguished Young Scientists of Jiangsu Province (Grant BK20190013) and the National Natural Science Foundation of China (Grants 51978154, 52008099, and 51608258), and Natural Science Foundation of Jiangsu Province (Grant BK20200369).

References

Cao, Y., and M. L. Wang. 2010. "Cable stress monitoring for a cable stayed bridge." In *Proc., 5th European Workshop on Structural Health Monitoring*, 1196–1201. Naples, Italy: Alenia Aeronautica, CIRA, DAppolonia S p A, US AF Off Sci Res, Univ Pavia, Natl Res Council, Inst Composite & Biomed Mat.

Chaudhuri, T., D. Zhai, Y. C. Soh, H. Li, and L. Xie. 2018. "Thermal comfort prediction using normalized skin temperature in a uniform built environment." *Energy Build.* 159: 426–440. https://doi.org/10.1016/j.enbuild.2017.10.098.

Chen, C. C., W. H. Wu, C. Y. Liu, and G. Lai. 2017. "Elimination of environmental temperature effect from the variation of stay cable force based on simple temperature measurements." *Smart Struct. Syst.* 19 (2): 137–149. https://doi.org/10.12989/sss.2017.19.2.137.

Chen, Z., T. J. Feng, and Q. C. Meng. 1999. "The application of wavelet neural network in time series prediction and system modeling based on multiresolution learning." In Vol. 1 of *IEEE Int. Conf. on Systems, Man, and Cybernetics*, 425–430. Piscataway, NJ: IEEE.

Ding, Y. L., Y. Deng, and A. Q. Li. 2010. "Study on correlations of modal frequencies and environmental factors for a suspension bridge based on improved neural networks." *Sci. China* 9: 195–203.

Ding, Y. L., and A. Q. Li. 2011. "Temperature-induced variations of measured modal frequencies of steel box girder for a long-span suspension bridge." *Int. J. Steel Struct.* 11 (2): 145–155. https://doi.org/10.1007/s13296-011-2004-4.

Ge, J. Y., and M. B. Su. 2016. "Simulation method for cable damage of cable-stayed bridge and its effect on cable tension and deflection distribution." [In Chinese.] *China Railway Sci* 37 (3): 30–37.

Gers, F. A., and J. Schmidhuber. 2000. "Recurrent nets that time and count." In Vol. 3 of *IEEE-INNS-ENNS Int. Joint Conf. on Neural Networks*, 189–194. Piscataway, NJ: IEEE.

Graves, A., M. Liwicki, F. Santiago, R. Bertolami, H. Bunke, and J. Schmidhuber. 2009. "A novel connectionist system for unconstrained handwriting recognition." *IEEE Trans. Pattern Anal. Mach. Intell.* 31 (5): 855–868. https://doi.org/10.1109/TPAMI.2008.137.

Jiao, Y., H. Liu, Y. Cheng, X. Wang, Y. Gong, and G. Song. 2014. "Fuzzy neural network-based damage assessment of bridge under temperature effect." *Math. Probl. Eng.* 2014: 418040. https://doi.org/10.1155/2014/418040.

Kaloop, M. R., and H. Li. 2014. "Multi input–single output models identification of tower bridge movements using GPS monitoring system." *Measurement* 47: 531–539. https://doi.org/10.1016/j.measurement.2013.09.046.

Kim, S., D. M. Frangopol, and M. Soliman. 2013. "Generalized probabilistic framework for optimum inspection and maintenance planning." *J. Struct. Eng.* 139 (3): 435–447. https://doi.org/10.1061/(ASCE)ST.1943-541X.0000676.

Kurkova, V. 1992. "Kolmogorov's theorem and multilayer neural networks." *Neural Networks* 5 (3): 501–506. https://doi.org/10.1016/0893-6080(92)90012-8.
Li, H., and J. P. Ou. 2015. "The state of the art in structural health monitoring of cable-stayed bridges." *J. Civ. Struct. Health Monit.* 6 (1): 43–67. https://doi.org/10.1007/s13349-015-0115-x.
Li, T., T. Wu, and Z. Liu. 2020. "Nonlinear unsteady bridge aerodynamics: Reduced-order modeling based on deep LSTM networks." *J. Wind Eng. Ind. Aerodyn.* 198: 104116. https://doi.org/10.1016/j.jweia.2020.104116.
Li, X., and X. Chen. 2019. "Influence of cable tension on the mechanical properties of cable-stayed bridge." *Jordan J. Civ. Eng.* 13 (1): 158–169.
Liu, G., Y. M. Shao, Z. M. Huang, and X. J. Zhou. 2010. "A new method to separate temperature effect from long-term structural health monitoring data." *Eng. Mech.* 27 (3): 55–61.
Malomo, D., N. Scattarreggia, A. Orgnoni, R. Pinho, M. Moratti, and G. M. Calvi. 2020. "Numerical study on the collapse of the Morandi bridge." *J. Perform. Constr. Facil.* 34 (4): 04020044. https://doi.org/10.1061/(ASCE)CF.1943-5509.0001428.
Seep, H., and S. Jurgen. 1997. "Long short-term memory." *Neural Comput.* 9 (8): 1735–1780. https://doi.org/10.1162/neco.1997.9.8.1735.
Sun, L. M., Z. Q. Shang, and Y. Xia. 2019. "Development and prospect of bridge structural health monitoring in the context of big data." [In Chinese.] *China J. Highway Transp.* 32 (11): 1–20.
Sun, L., Z. Shang, Y. Xia, S. Bhowmick, and S. Nagarajaiah. 2020. "Review of bridge structural health monitoring aided by big data and artificial intelligence: From condition assessment to damage detection." *J. Struct. Eng.* 146 (5): 04020073. https://doi.org/10.1061/(ASCE)ST.1943-541X.0002535.
Sun, Y. Q., and Z. Z. Zhao. 2019. "Real-time seperation of temperature effect on dynamic strain monitoring and moving load identification of bridge structure." *Eng. Mech.* 36 (2): 186–194.
Wang, G. X., and Y. L. Ding. 2019. "Reliability estimation of horizontal rotation at beam end of long-span continuous truss bridge affected by temperature gradients." *J. Perform. Constr. Facil.* 33 (6): 04019061. https://doi.org/10.1061/(ASCE)CF.1943-5509.0001336.
Wang, G. X., and J. H. Ye. 2019. "Localization and quantification of partial cable damage in the long-span cable-stayed bridge using the abnormal variation of temperature-induced girder deflection." *Struct. Control Health Monit.* 26 (1): e2281. https://doi.org/10.1002/stc.2281.
Williams, R. J., and J. Peng. 1990. "An efficient gradient-based algorithm for on-line training of recurrent network trajectories." *Neural Comput.* 2 (4): 490–501. https://doi.org/10.1162/neco.1990.2.4.490.
Xu, X., Q. Huang, Y. Ren, D. Y. Zhao, J. Yang, and D. Y. Zhang. 2019. "Modeling and separation of thermal effects from cable-stayed bridge response." *J. Bridge Eng.* 24 (5): 04019028. https://doi.org/10.1061/(ASCE)BE.1943-5592.0001387.
Xu, Y. L., B. Chen, C. L. Ng, K. Y. Wong, and W. Y. Chan. 2010. "Monitoring temperature effect on a long suspension bridge." *Struct. Control Health Monit.* 17 (6): 632–653. https://doi.org/10.1002/stc.340.
Yang, D. H., T. H. Yi, H. N. Li, and Y. F. Zhang. 2018a. "Correlation-based estimation method for cable-stayed bridge girder deflection variability under thermal action." *J. Perform. Constr. Facil.* 32 (5): 04018070. https://doi.org/10.1061/(ASCE)CF.1943-5509.0001212.
Yang, D. H., T. H. Yi, H. N. Li, and Y. F. Zhang. 2018b. "Monitoring and analysis of thermal effect on tower displacement in cable-stayed bridge." *Measurement* 115: 249–257. https://doi.org/10.1016/j.measurement.2017.10.036.
Yang, H., Z. Sun, X. P. Liu, W. Zhu, and Y. Wang. 2014. "Separation of bridge temperature deflection effect based on M-LS-SVM." *J. Vib. Shock* 33 (1): 71–76+88.
Ye, X. W., T. Jin, and C. B. Yun. 2019. "A review on deep learning-based structural health monitoring of civil infrastructures." *Smart Struct. Syst.* 24 (5): 567–585. https://doi.org/10.12989/sss.2019.24.5.567.
Yoshua, B., S. Patrice, and F. Paolo. 1994. "Learning long-term dependencies with gradient descent is difficult." *Neural Networks* 5 (2): 157–166.
Zhang, Q. 1992. "Wavelet networks." *IEEE Trans. Neural Networks* 3 (6): 889–898. https://doi.org/10.1109/72.165591.
Zhao, H. W., Y. L. Ding, A. Q. Li, Z. Z. Ren, and K. Yang. 2020a. "Live-load strain evaluation of the prestressed concrete box-girder bridge using deep learning and clustering." *Struct. Health Monit.* 19 (4): 1051–1063. https://doi.org/10.1177/1475921719875630.
Zhao, H. W., Y. L. Ding, A. Q. Li, W. Sheng, and F. Geng. 2020b. "Digital modeling on the nonlinear mapping between multi-source monitoring data of in-service bridges." *Struct. Control Health Monit.* 27 (11): e2618. https://doi.org/10.1002/stc.2618.
Zhou, X. G., and X. H. Zhang. 2019. "Thoughts on the development of bridge technology in China." *Engineering* 5 (6): 1120–1130. https://doi.org/10.1016/j.eng.2019.10.001.
Zhou, Y., and L. Sun. 2019a. "A comprehensive study of the thermal response of a long-span cable-stayed bridge: From monitoring phenomena to underlying mechanisms." *Mech. Syst. Sig. Process.* 124: 330–348. https://doi.org/10.1016/j.ymssp.2019.01.026.
Zhou, Y., and L. Sun. 2019b. "Insights into temperature effects on structural deformation of a cable-stayed bridge based on structural health monitoring." *Struct. Health Monit.* 18 (3): 778–791. https://doi.org/10.1177/1475921718773954.
Zhu, J. S., and Q. L. Meng. 2017. "Effective and fine analysis for temperature effect of bridges in natural environments." *J. Bridge Eng.* 22 (6): 04017017. https://doi.org/10.1061/(ASCE)BE.1943-5592.0001039.